ISSN 2032-6653

Battery Thermal Management Design Modeling

Gi-Heon Kim* and Ahmad Pesaran*

Battery thermal management is critical in achieving performance and the extended life of batteries in electric and hybrid vehicles under real-driving conditions. Appropriate modeling for predicting thermal behavior of battery systems in vehicles helps to make decisions for improved design and shortens the development process. For this paper, we looked at the impact of cooling strategies with air and direct/indirect liquid cooling. The simplicity of an air-cooling system is an advantage over a liquid-cooling system. In addition to its intrinsically lower heat transfer coefficient, another disadvantage of air cooling is that the small heat capacity of air makes it difficult to accomplish temperature uniformity inside a cell or between cells in a module. Liquid-cooling is more effective in heat transfer and takes up less volume, but the added complexity and cost may outweigh the merits. The surface heat transfer coefficient, h, and the blower power for air cooling are sensitive to the hydraulic diameter of the cooling channel (D_h). However, because of the added thermal resistances, h evaluated at cell surface is not as sensitive to the variation of D_h in an indirect (water/glycol jacket) cooling system. Due to the high heat transfer coefficient at small D_h, direct liquid cooling using dielectric mineral oils may be preferred in spite of high pressure loss in certain circumstances such as in highly transient large heat generating battery systems. In general, air-cooling should be considered first, as the power demand increases with heavier vehicles and more aggressive driving, water/glycol jacket cooling should be considered next. Results of computational fluid dynamics model simulation imply that capturing the internal heat flow paths and thermal resistances inside a cell using a sophisticated three-dimensional cell model is important for more accurate prediction of cell/battery thermal behaviors. This paper identified analyses and approaches that engineers should consider when they design a battery thermal management system for vehicles.

Keywords: Hybrid Electric Vehicle, HEV, Battery Model, Thermal Management System

1. INTRODUCTION

Temperature greatly affects the performance and life of batteries, so battery thermal control must be used in electric, hybrid, and plug-in hybrid electric vehicles under real-driving conditions. In recent years, automakers and their battery suppliers have paid increased attention to battery thermal management, especially with regard to life cycle and related warranty costs.

The basic performance of the management system is dictated by the thermal design of each cell and module. Gu and Wang [1] developed a two-dimensional thermal and electrochemical coupled lithium-ion cell model to understand the temperature effect on electrochemistry and vice versa. Srinivasan and Wang [2] examined the methodology of using experimental data, instead of an electrochemical model, to determine cell heat generation rate. But their two-dimensional approach was limited to a simple one-set single cell, which cannot address various thermal conditions and geometrical effects. Pesaran et al. [3] and Bharathan et al. [4] have demonstrated the utility of three-dimensional models for improving the current and temperature distributions in batteries by including the geometrical details in model domains. However, these papers did not consider the detailed electrochemistry. Al-Hallaj et al. [5] presented phase change material (PCM) thermal management as a potential option for high-power applications.

Fig. 1 presents the concept diagram showing the battery thermal management modeling process at the National Renewable Energy Laboratory (NREL). The cell characteristics (e.g., chemistry, form-factor, dimension, and materials), operating conditions (e.g., power load profiles from the vehicle, and ambient

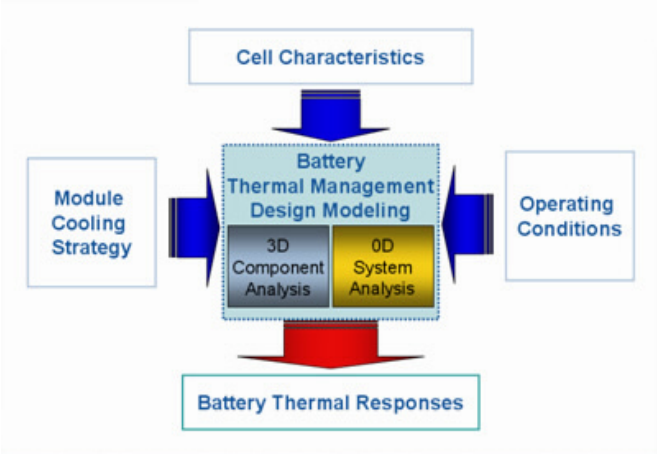

Fig. 1 Working flow diagram for battery thrmal management modeling process at NREL

*National Renewable Energy Laboratory, 1617 Cole Blvd., Golden, Colorado 80401 USA, email: gi_heon_kim@nrel.gov;

© 2007 WEVA Journal, pp. 126-133

ISSN 2032-6653

temperatures), module/pack cooling strategy (e.g., coolant type and mass flow rates, coolant channel design, and temperature duty cycle) are all input to the NREL's battery thermal management design model. The model uses these inputs for component and system analysis to predict the thermal response of the design. Then, the promising modifications to the design can be evaluated to determine the optimum solution while considering factors such as cost, volume, mass, and maintenance issues.

The presented study focused on examining the viable cooling strategies. In order to find a high-performance and cost-effective cooling system, it is necessary to evaluate system thermal response and its sensitivity as a function of controllable system parameters. This paper identifies analyses and approaches that engineers should consider when they design a battery thermal management system for vehicles.

2. ANALYSIS AND RESULTS

A typical parallel cell cooling system was investigated using fully developed channel relations and computational fluid dynamics. Fig. 2 presents the schematics of a system. Pressure loss in coolant channel (ΔP), coolant temperature change between channel inlet and outlet (ΔT_1), and temperature difference between cell surface and coolant mean temperature (ΔT_2) are chosen for the system responses of interest. ΔP and the coolant flow rate are critical factors determining the required pump/blower power and size. ΔT_1 is a parameter indicating the cell temperature uniformity that possibly could be achieved. ΔT_2 is closely related to the heat transfer coefficient, h, and shows how much the cell temperature would differ from the coolant temperature or how fast the heat would be transferred at a given temperature difference. On the other hand, the maximum cell surface temperature relative to coolant inlet temperature, $\Delta T_{max} = \Delta T_1 + \Delta T_2$, can be used as a parameter for controlling the limit of cell temperature tolerance.

Note that the cell internal temperature distribution and the maximum temperature at cell surface depend on the thermal paths and resistance distributed inside a cell. Therefore, the shapes, materials, thermal connectivity of cell components, and location of heat transfer surfaces are important for predicting cell internal temperatures. Detailed investigations into this topic

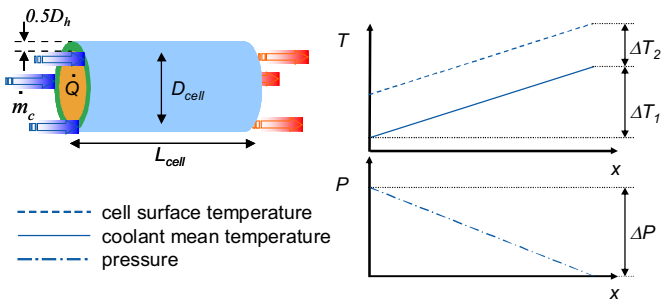

Fig. 2 Schematics of a typical parallel cell cooling system and system responses

have been covered in separate studies [3,4]. The effects of using different types of coolants were examined here (See Table 1). We selected coolant mass flow rate ($\dot{m}_c$) and the hydraulic diameter of coolant channels (D_h) as system control parameters. In this study, the cell with a 50-mm diameter, a 100-mm length, and 2 W heat generation was chosen for base case cell.

2.1. Fully Developed Flow Analysis

Even though the heat transfer is enhanced in a turbulent flow regime, the required blower power greatly increases with laminar to turbulence flow transition. Therefore, many heat exchanger applications are designed to be operated at laminar flow regimes. If the channel gap is small enough compared with the cell diameter, the following fully developed laminar flow relations can be applied to the presented system.

$$c_f \mathrm{Re} = 24$$
$$\mathrm{Nu} = 5.385 \qquad (1)$$

where Re= VD_h/ν, Nu= hD_h/k. c_f is friction coefficient. The Nuselt number is evaluated for constant heat flux wall boundary conditions.

Channel Pressure and Power Losses Fig. 3 (a) shows the channel pressure losses per unit mass flow rate ($\Delta P/\dot{m}_c$) as a function of coolant channel hydraulic diameter for different coolants. Due to the large difference in kinematic viscosity, ΔP varies in very different ranges for each coolant fluid. ΔP is directly proportional to fluid kinematic viscosity (ν) and coolant mass flow rate ($\dot{m}_c$). If the cell diameter is much larger than D_h, ΔP becomes inversely proportional to D_h^3. Therefore the channel pressure loss changes are very sensitive to D_h when it is small, especially for the high-kinematic viscosity fluids.

$$\Delta P \sim \frac{\dot{m}_c \nu}{D_h^3}$$

$$\frac{\partial \Delta P}{\partial D_h} \sim -\frac{\dot{m}_c \nu}{D_h^4} \qquad (2)$$

Flow power requirements to overcome the channel friction loss were normalized by the square of coolant mass flow rate and compared for the different coolant systems in Fig. 3(b). Due to the much smaller fluid density and consequently larger volumetric flow rate at

Table 1 Properties of coolants typically used in battery cooling systems

Property \ Coolant	Air	Mineral Oil	Water/Glycol
Density ρ (kg/m^3)	1.225	924.1	1069
Specific Heat c_p ($J/kg\ K$)	1006.43	1900	3323
Thermal Conductivity k ($W/m\ K$)	0.0242	0.13	0.3892
Kinematic Viscosity ν (m^2/s)	1.461e-5	5.6e-5	2.582e-6

© 2007 WEVA Journal, pp. 126-133

ISSN 2032-6653

given mass flow rate, the air-cooling system requires much higher flow power for compensating channel friction loss than the liquid coolant systems at the given coolant mass flow rate and channel height. However, in liquid-cooling systems, not only the coolant channel friction loss but also the system manifold friction head and the static pressure head make a significant contribution to the required pumping power.

Temperature Differences Variations of ΔT_1 and ΔT_2 are shown for the coolant mass flow rate and the hydraulic diameter of coolant channel respectively in Fig. 4. To achieve temperature uniformity through a cell, it is preferred to keep coolant temperature change (ΔT_1) in the channel as small as possible. ΔT_1 is inversely proportional to coolant heat capacity flow rate. Therefore, for low flow rate cooling, a little change in flow rate can greatly affect the coolant temperature change, and consequently cell temperatures (especially when air is used for the heat transfer medium that has small c_p as compared in Fig. 4). Water/glycol is the most preferred among the tested coolant materials for achieving temperature uniformity of cell/pack because of its large specific heat.

$$\Delta T_1 \sim \frac{1}{\dot{m}_c c_p} \qquad (3)$$

$$\frac{\partial \Delta T_1}{\partial \dot{m}} \sim -\frac{1}{c_p}\frac{1}{\dot{m}_c^{\,2}}$$

Temperature difference between coolant flow and cell surface, ΔT_2, is linear to D_h with the slope proportional to 1/k as shown in Fig. 4. The 0.7-mm jacket wall thickness and 0.05-mm air layer were considered between the cell surface and water/glycol coolant channel. Due to small thermal conductivity of air, ΔT_2 rapidly increases with D_h in air cooling. Therefore, to achieve a small ΔT_2 (or large heat transfer coefficient, h), reducing the hydraulic diameter of the channel is critical for air cooling. On the other hand, ΔT_2 is not very sensitive to variations of D_h in the water/glycol cooling system because of the relatively large thermal conductivity.

$$\Delta T_2 \sim \frac{1}{k} D_h + const \qquad (4)$$

where *const* is 0 for direct-contact cooling in the relation shown at Eq 4.

The ΔT_2 curve shown in Fig. 4 also implies the heat transfer coefficient, h, which is inversely proportional to ΔT_2. h is plotted as a function of D_h in Fig. 5. High h lowers ΔT_2 to reduce cell temperature. In unsteady heat transfer, high h means fast heat removal or addition from small temperature displacement, limiting the peak temperature of the cell. Therefore, high h smoothes out the cell temperature oscillations under transient heat generating conditions. The heat transfer coefficient evaluated at cell surface for water/glycol jacket cooling, due to added thermal resistances between coolant and cell, greatly decreases compared with the value it would be if direct-contact cooling. The reduction is greater at

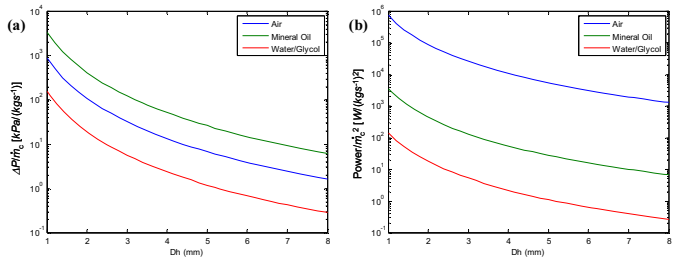

Fig. 3 (a) Channel pressure loss per unit mass flow rate as a function of the coolant channel hydraulic diameter. (b) Flow power requirement for pressure loss normalized by square of mass flow rate as a function of the coolant channel hydraulic diameter.

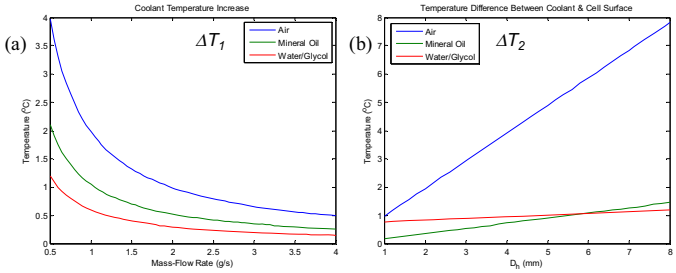

Fig. 4 (a) Variation of coolant temperature change inside a system as a function of coolant mass flow rate. (b)Variation of temperature difference between coolant and cell surface as a function of hydraulic diameter of coolant channel.

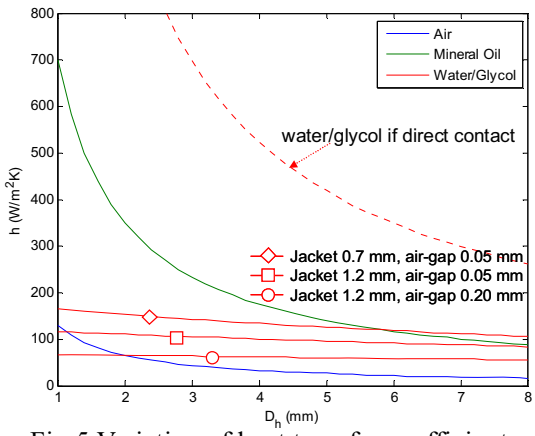

Fig.5 Variation of heat transfer coefficient as a Function of coolant channel hydraulic diameter.

small D_h. So, the direct liquid cooling using mineral oil shows much higher h values than the other coolants at D_h <2~3 mm in the presented case. In spite of large pressure losses due to large ν and small D_h in this operating region, mineral oil cooling may be preferred for its high-heat transfer coefficient in certain conditions.

Contours of maximum cell surface temperature relative to coolant inlet temperature, ΔT_{max} (=ΔT_1+ ΔT_2) are plotted as a function of coolant mass flow rate and hydraulic diameter of coolant channels for different coolant systems in Fig. 6. The values of ΔT_{max} in the air system are much higher compared with other fluid systems due to its small heat capacity and thermal conductivity. Contour lines for the air system, Fig. 6(a),

© 2007 WEVA Journal, pp. 126-133

ISSN 2032-6653

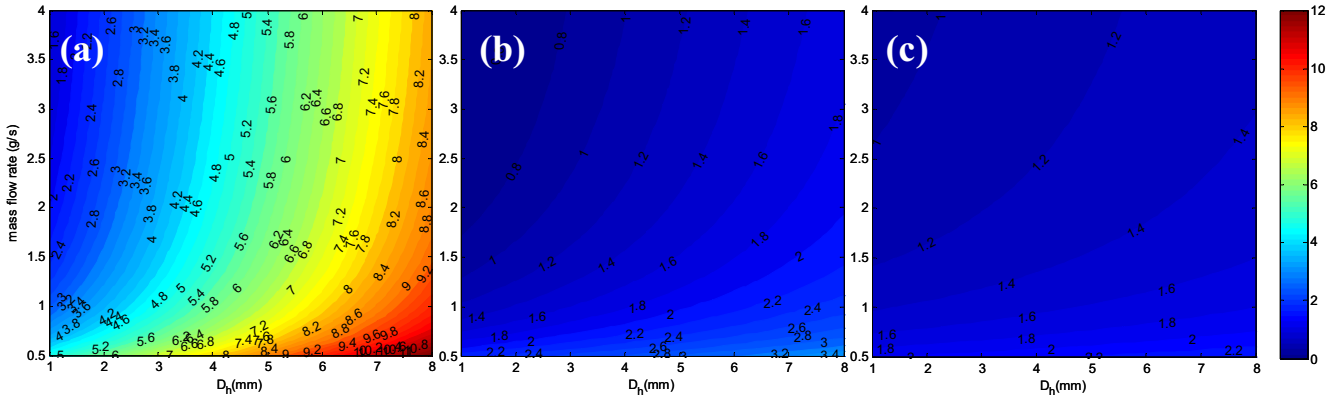

Fig. 6 Contours of maximum cell surface temperature relative to coolant inlet temperature

are dense and mostly aligned vertically at $\dot{m}_c > \sim 1$ g/s. This means that ΔT_{max} is dominated by and sensitive to D_h in this operating region. On the other hand, the water/glycol jacket cooling system [Fig. 6(c)] contour lines are almost horizontal at $\dot{m}_c < \sim 2$ g/s, and the line density is relatively sparse at $\dot{m}_c > \sim 2$ g/s. This means that ΔT_{max} is not very sensitive to D_h, and that ΔT_{max} would not be a strict limiting design factor of the water/glycol system. The lowest value of ΔT_{max} appears in the mineral oil direct-contact cooling system (Fig. 6(b)) with a small D_h and large $\dot{m}_c$ operating region. Note that large pressure loss accompanies in that operation region.

System Operation Parameter Optimization An example of confining the operation zone to given conditions is shown in Fig. 7. By drawing contour lines of required conditions, possible operating zones can be found. The colored area shown in Fig. 7 represents the operating zone satisfying Re<2300, ΔP <110 Pa, ΔT_{max} <4.5°C and ΔT_1<1.5°C in an air-cooling system. Laminar restriction of the Reynolds number is to avoid excessive friction loss due to turbulence flow transition. Point A is the operating point for achieving maximum h for given conditions. B is the lowest ΔT_{max} operating point, and C is the minimum pressure loss (ΔP) operating point.

2.2 Computational Fluid Dynamics Analysis

Air Cooling An operating point (D_h , $\dot{m}_c$) = (2.2 mm, 1.33 g/s), which is close to point A in Fig. 7, the maximum h operating point satisfying given limiting conditions, was selected and simulated for the air-cooling system using an axisymmetric computational fluid dynamics (CFD) model. The model geometry and mesh are presented in Fig. 8. The model includes internal cell component materials and geometries. The cell core winding was treated as a continuous material having orthotropic properties according to layer directions. As specified previously, the cell is 50 mm in diameter, 100 mm in length, and generates heat with a rate of 2 W at its core. Inlet air temperature was set to 35°C. The other surfaces, except the channel/cell interface, were set as thermally adiabatic boundaries.

Fig. 9 shows temperature distribution contours of the cell and cooling air. In the upper frame of the figure, radial-direction length scale is exaggerated to see the thermal development in the air channel. Cell surface temperature constantly increases in the axial direction as coolant air temperature increases. However, cell internal temperature distribution is determined by the thermal paths and thermal resistances inside a cell. The maximum temperature of 38.4°C appears on the cell axis a little bit downstream from the cell center in the presented cell specification.

Axial distribution of the airflow mean temperature, cell surface temperature, and cell center-line temperature are presented in Fig. 10. Coolant air temperature change, ΔT_1, is computed as 1.5°C. The maximum cell surface temperature relative to inlet air temperature, ΔT_{max}, is 2.9°C at the channel outlet. The highest battery temperature appears in the middle of the centerline of the cell and displaced from coolant inlet temperature by 3.4°C. Due to entrance effect, air temperature rapidly increases near the channel inlet. In the entrance region, the radial profiles of temperature and velocity at the cell/coolant interface have steep gradients representing higher heat flux and wall friction. Entrance effect is more clearly seen on the axial distribution of the heat transfer coefficient (h) and heat flux shown in Fig. 11.

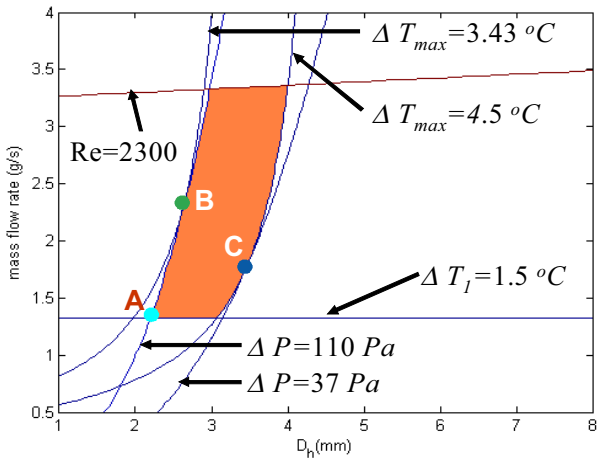

Fig. 7 Confining the operation zone and parameter optimization to given conditions

© 2007 WEVA Journal, pp. 126-133

ISSN 2032-6653

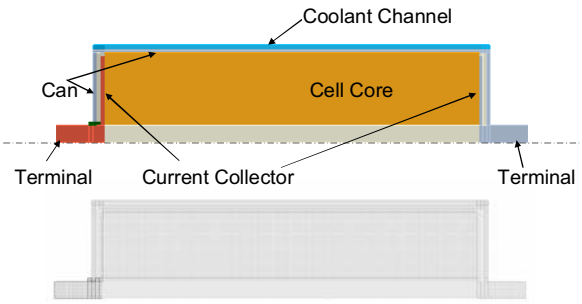

Fig. 8 Model geometry and mesh representing an axisymmetric cylindrical cell

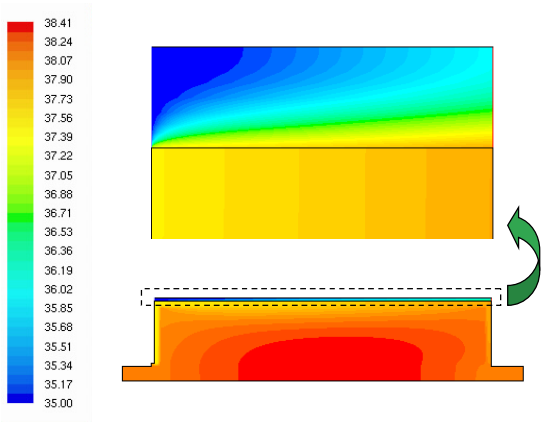

Fig. 9 Temperature distribution contours of the cell and the air coolant channel (top: expanded view near can surface and coolant channel)

The heat transfer coefficient, h, at the cell surface has a larger value near the channel inlet, and consequently, so does the heat flux. As the flow approaches fully developed, the value of h converges to the constant value, 56.23 W/m^2K, which is slightly lower than the predicted value, 59.24 W/m^2K, using the relations shown in Eq. 1. However, the mean value of h over the heat transfer surface has a little bit higher value, 60.96 W/m^2K, due to the entrance zone effect. One of the reasons for this discrepancy comes from the fact that heat flux distribution is not quite constant along the axial distance.

System response parameters from different prediction methods are presented in Table 2. Even though ΔP is predicted to be a little bit higher in CFD analysis due to the entrance effect, the parameters are generally well matched between the prediction methods except for the maximum cell surface temperatures. The disagreement of ΔT_{max} mainly originates from the fact that CFD analysis can capture the axially decreasing heat flux from cell to air, which makes the axial gradient of the cell surface temperature smaller than that of the air temperature. This is because high conductivity materials inside a cell, such as the aluminum can, would transfer internal heat flow to make cell temperature more even. This result strongly implies that capturing the internal heat flow paths and thermal resistances inside a cell are important for the improved

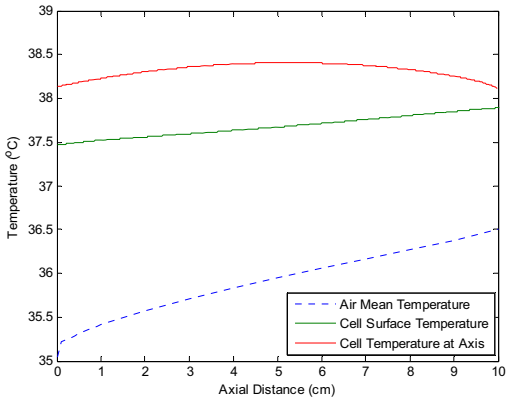

Fig. 10 Axial distribution of air flow mean temperature, cell surface temperature and cell center-line temperature

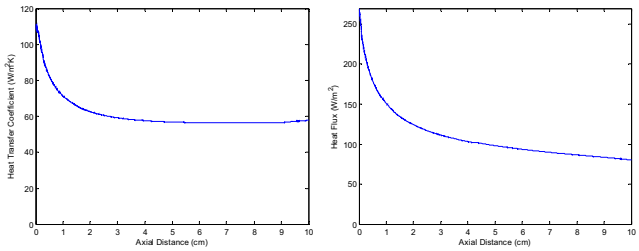

Fig. 11 Axial distribution of heat transfer coefficient and heat flux

prediction of cell/battery thermal behaviors.

Air and Water/Glycol Cooling Comparison Cooling of a larger cell that has a 50-mm diameter, 200-mm length, and generates heat with a rate of 4 W at the cell core was simulated for a direct air-cooling system and a water/glycol-jacket cooling system in order to contrast the characteristics of each system. Reducing channel height greatly increases heat transfer coefficient at cell surface in a direct-contact, air-cooling system. But reducing the channel height is limited by the channel friction loss, which increases sensitively with decreasing D_h for a given coolant flow rate. On the other hand, in an indirect water/glycol liquid-cooling system, channel height is not a sensitive factor affecting heat transfer coefficient at the cell surface as it is in air systems, even though water/glycol channel friction loss is not as significant in magnitude as in air for a given coolant mass flow rate. But it is still recommended in a liquid-cooling system to use a small gap coolant channel to reduce system weight and volume by

Table 2 System response parameters - Two different prediction methods

	ΔP [Pa] channel pressure loss	ΔT_1 [°C] coolant temperature change	ΔT_{max} [°C] maximum cell surface temperature to inlet air	ΔT_{cell} [°C] maximum cell internal temperature to inlet air	$\bar{h}$ [W/m²K] mean heat transfer coefficient
Fully Developed Flow Relations with Constant Heat Flux	109.1	1.49	3.64	N/A	59.24
CFD	114.2	1.50	2.89	3.41	60.96

© 2007 WEVA Journal, pp. 126-133

ISSN 2032-6653

minimizing the amount of coolant in a system operated at a given coolant flow rate. CFD analyses were carried out for a direct air-cooling system operated at (D_h , $\dot{m}_c$) = (2.2 mm, 1.33 *g/s*) and for a water/glycol-jacket cooling system at (D_h , $\dot{m}_c$) = (4.0 mm, 1.70 *g/s*). Inlet coolant temperatures were set at 35°C. The results indicate that due to the large differences of coolant velocity and kinematic viscosity between the two systems, the air-cooling system needs to compensate for a much larger pressure loss than the water/glycol liquid-cooling system (221 *Pa* versus 7.68 *Pa*).

Temperature distribution contours are shown for comparison in Fig. 12. Even though the rate of heat removal from cell to coolant is the same for the two compared systems, airflow is rapidly heated compared with water/glycol due to the small heat capacity of air flow. In addition, the difference between coolant mean temperature and cell surface temperature is larger in the air-cooling system because of the smaller heat transfer coefficient. Therefore, not only the maximum temperature but also the temperature nonuniformity inside a cell are larger in the air-cooling system than in the water/glycol system. Temperature contour-lines are distributed similarly inside a cell in both cases. This implies that internal heat flows are similar in both systems, and consequently, that the internal heat paths and the thermal resistances are determining the relative temperature distribution inside a cell.

Axial temperature profiles of the air-cooling system and the water/glycol system are compared in Fig. 13 (a). Compared with the water/glycol liquid cooled cell, the maximum temperature on the cell axis in the air-cooled cell appears near the channel exit. A larger temperature difference between each end of the cell shifts the maximum temperature location further downstream. Heat transfer coefficients at cell surfaces are plotted in Fig. 13 (b) for both systems.

$$h = \frac{q''}{T_{cell_surf} - \overline{T}_{coolant}} \qquad (5)$$

Thermal resistances of the jacket wall and air-gap layer, between the channel coolant and the cell surface, were considered to evaluate the heat transfer coefficient of the water/glycol cooling system. Temperature displacement between the channel surface and the cell surface in the water/glycol cooled cell shown in Fig. 13 (a) is due to these added thermal resistances. The higher heat transfer coefficient of the water/glycol system leads to a smaller temperature difference between the coolant and cell surface as shown in Fig. 13 (a) and Eq. 5. Even though the cell temperatures are distributed in different ranges for each system, the magnitudes of temperature differences between the cell center axis and the cell surface of the air-cooled cell and the water/glycol cooled cell are similar because the same cell specifications are assumed for both cases.

Although, a serial-cooling system may provide simplicity over a parallel cooling system because of for its simpler of manifolding flow distribution, parallel cooling provide a better cell to cell temperature

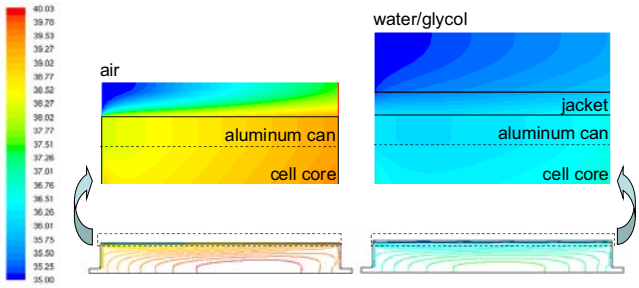

Fig. 12 Comparison of temperature distribution contours between air cooled cell and water/glycol cooled cell

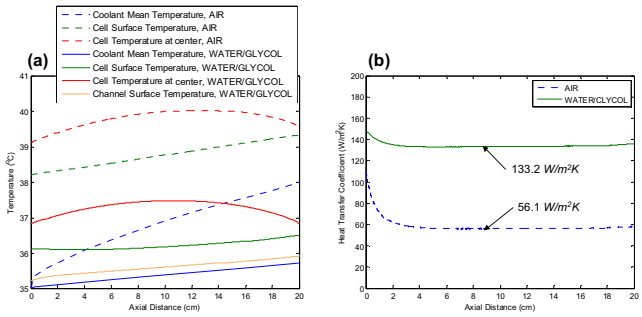

Fig. 13 (a) Axial profiles of temperatures, and (b) heat transfer coefficients at cell surfaces

uniformity. The CFD simulation results shown in Fig. 13 are simply extended to a six-cell, serial-cooling system and presented in Fig. 14. Other heat exchanges among the cells, such as conduction through electric connectors, are ignored. Cell temperature differences in a module more rapidly increase in the air-cooling system proportional to the number of cells connected serially with the coolant channel. Cell-to-cell temperature imbalance mainly comes from the coolant temperature change in coolant channels. Due to the low heat capacity of air, it is difficult to accomplish temperature uniformity inside a cell or between the cells in a module using air for cooling large or high-heat generating cells.

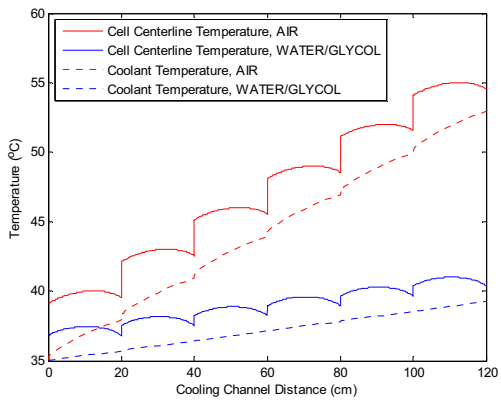

Fig. 14 Extended temperature profiles for a six-cell serial cooling system

© 2007 WEVA Journal, pp. 126-133

ISSN 2032-6653

Transient Analysis In order to investigate the time-dependent thermal response of battery cooling systems, transient CFD analyses were carried out with a cell specified in Fig. 8. An air-cooling system; a mineral oil, direct liquid-cooling system; and a water/glycol jacket cooling were compared. The systems were operated with the same channel geometry and coolant mass flow rate, (D_h , $\dot{m}_c$) = (2.2 mm, 1.33 *g/s*). Initially, each system was in steady state with a heat generation rate of 2 *W*. A system was heated with sudden heat generation (50 *W*) for 2 min. Then, the cell was cooled down to the initial steady-state conditions. Coolant inlet temperatures were kept constant at 35°C.

Using steady state fully developed relationships shown in Eq.1, channel pressure losses (ΔP) are predicted as 109.1 *Pa*, 418.3 *Pa*, and 18.27 *Pa* for the air system, the mineral oil system, and the water/glycol system respectively. On the other hand, heat transfer coefficients are predicted as 59.24 W/m^2K for the air-cooled surface, 318.2 W/m^2K for the mineral oil cooled surface, and 150.8 W/m^2K for an effective heat transfer coefficient at the water/glycol jacket cooling cell surface. The mineral oil, direct-contact, liquid-cooling system is expected to have a much higher heat transfer coefficient than the other coolant systems (direct air and indirect water/glycol) when it is operated at a small channel (D_h) and large coolant flow rate ($\dot{m}_c$) at the expense of high pressure loss in the coolant channel. The water/glycol system has a larger heat capacity flow rate ($\dot{m}_c c_p$, 4.42 *J/Ks*) than the mineral oil system (2.53 *J/Ks*) or airflow system (1.34 *J/Ks*), which means it can remove the suddenly released heat from the cell with a smaller increase of coolant temperature. The simulation results showing the transient effect of using high *h* and a high heat capacity coolant system are presented in Fig. 15 and Fig. 16.

The heat transfer rates from the cell to the coolant are compared in Fig. 15. Due to the highest heat transfer coefficient, released heat is most quickly removed from the mineral-oil-cooled cell. On the other hand, the heat rejecting amount in water/glycol system is comparable with the mineral oil cooling system in spite of its smaller heat transfer coefficient. This is because the temperature potential is larger in the water/glycol system for a lower coolant temperature. In a high *h* and high $\dot{m}_c c_p$ system, a large amount of heat can be transferred from cell to coolant with a small temperature increase of the cell while the coolant temperature does not change much.

Time variations of the mean temperature within the cell core and the mean temperature of the coolant outlet are shown in Fig. 16 for the air-, mineral-oil-, and water/glycol-jacket cooling systems. Since the heat rejection rates of both liquid-cooling systems are similar to the given conditions, as it is shown in Fig. 15, the average cell temperature variation profiles are also similar. In both the liquid-cooling systems, the peak temperature is lower and the cooldown time is shorter than in the air-cooling system. Note that the mineral oil system cooled down a little bit faster than the

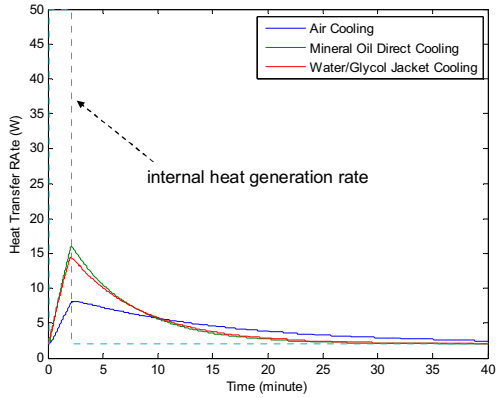

Fig. 15 Time variation of heat transfer rates from the cell to the coolant

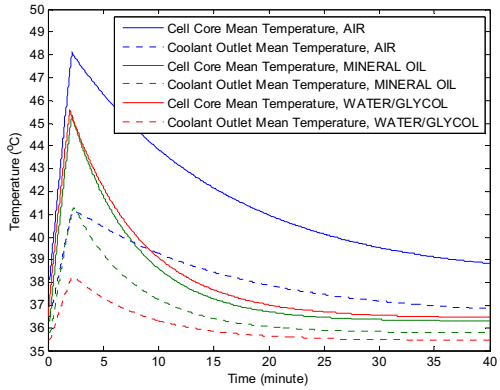

Fig. 16 Time variations of mean temperature of the cell core and the coolant outlet temperature

water/glycol cooled cell, even though the coolant temperature of mineral oil system is higher than the temperature of water/glycol. The results imply that a high *h* system (and high $\dot{m}_c c_p$ system, if possible) is preferred for limiting the maximum peak temperature of a cell and damping out the temperature oscillation in highly transient heat generating battery systems.

3. CONCLUSIONS

To achieve performance and cost-effective cooling of a battery module/pack for electric or hybrid vehicles, the system thermal responses and their sensitivities are evaluated as a function of controllable system parameters (e.g., D_h and $\dot{m}_c$). For given cell specifications, different types of coolant are examined: air cooling, direct-contact liquid cooling using mineral oil, and (indirect) water/glycol jacket cooling.

The simplicity of an air-cooling system is an advantage over a liquid-coolant system. Air cooling could have less mass, has no potential for leaks, needs fewer components, and could cost less. However, the heat transfer coefficient (*h*) of an air-cooling system is lower than that of other coolant systems. Another drawback of an air system comes from its small heat capacity. Due to the small heat capacity of air, it is difficult to accomplish temperature uniformity inside a cell or between the cells in a module for large format

© 2007 WEVA Journal, pp. 126-133

ISSN 2032-6653

application. The temperature difference between coolant air and cell surface (ΔT_2) is sensitive to variations of D_h due to small heat conductivity of air. The heat transfer coefficient (h) is inversely proportional to D_h, while pressure loss in channel (ΔP) is inversely proportional to D_h^3. Therefore, increasing h by reducing D_h is limited by the required blower power. Reducing coolant air temperature change inside a system (ΔT_1) by increasing flow rate ($\dot{m}_c$) is also limited by blower power and size.

Liquid-cooling is more effective in heat transfer and takes up less volume, but the added complexity and cost may outweigh the merits. Maintenance and repair of a liquid cooled pack is more involved and costlier. Indirect liquid cooling, with jackets, is easier to handle than direct liquid cooling.

A 50/50 water and glycol mixture for an indirect-cooling system, selected because of its low freezing temperature for vehicle applications, has much lower viscosity than dielectric mineral oil for direct liquid cooling. Therefore, increasing the coolant flow rate may not be as severely restricted by the pump power as it is in a mineral oil direct-cooling system. Water/glycol has a higher heat capacity. So, the coolant temperature change inside a system can be greatly reduced by using water/glycol as a heat transfer fluid in the system. This means that cell/module temperature uniformity can be effectively achieved even in a serial cooling system if the coolant paths are properly designed. Water/glycol mixtures generally have a higher thermal conductivity than oil. However, due to the added thermal resistance between coolant and cell surface, such as jacket wall and air gap, the effective heat transfer coefficient at the cell surface is greatly reduced. Because of the added thermal resistances, h is not as sensitive to the variation of D_h.

A mineral oil direct-contact liquid-cooling system has a much higher heat transfer coefficient (h) than the other coolant systems when it is operated at a small channel (D_h) and a large coolant flow rate ($\dot{m}_c$) at the expense of high pressure loss in coolant channel. So, a mineral-oil-cooling system may be preferred for limiting the maximum peak temperature of a cell and damping out the temperature oscillation in certain circumstances, such as in highly transient heat generating battery systems.

CFD analysis captured the axially decreasing heat flux from cell to air, which makes the axial gradient of cell surface temperature smaller than that of air temperature. This implies that capturing the internal heat flow paths and thermal resistances inside a cell using a sophisticated three-dimensional cell model is important for the improved prediction of cell/battery thermal behaviors.

ACKNOWLEDGEMENT

The U.S. Department of Energy (DOE) FreedomCAR and Vehicle Technologies Program funded this effort. We appreciate the support provided by Dave Howell and Tien Duong of DOE

REFERENCES

[1] W.B. Gu and C.Y. Wang, "Thermal and Electrochemical Coupled Modeling of a Lithium-Ion Cell, in Lithium Batteries ," ECS Proceedings, Vol.99-25 (1), pp.748-762, 2000.

[2] V. Srinivasan and C.Y. Wang, "Analysis of Electrochemical and Thermal Behavior of Li-Ion Cells," Journal of Electrochemical Society, Vol. 150, ppA98-A106, 2003.

[3] A. Pesaran, D. Bharathan, G.-H. Kim, A. Vlahinos, and T. Duong, "Improving Battery Design with Electro-Thermal Modeling", in 21st Electric Vehicle Symposium, Monte Carlo, Monaco, 2005.

[4] D. Bharathan, A. Pesaran, G.-H. Kim, and A. Vlahinos, "Electro-Thermal Modeling to Improve Battery Design", IEEE Vehicle Power and Propulsion Conference, IEEE, Chicago, IL USA, 2005.

[5] S. Al-Hallaj, et. al, "Novel PCM Thermal Management Makes Li-Ion Batteries A viable Option for High Power Applications," Battery Power Products and Technology Magazine, November 2004.

BIOGRAPHIES

Gi-Heon Kim has worked with the Advanced Vehicle Systems group at NREL since 2004. His recent research interests in advanced vehicle energy storage system tasks include development of a three-dimensional Li-Ion battery thermal abuse model and hybrid electric vehicle//electric vehicle battery thermal management system modeling. He has been working on various vehicle power system research topics, such as PEM fuel cell freeze start and alternative fuel based diesel after-treatment systems. His expertise is in heat and mass transfer, fluid mechanics, turbulence, combustion, reacting flows and computational fluid dynamics. Dr. Kim completed a Ph.D. in Mechanical Engineering from Colorado State University with research on performance improvement of natural gas engines. In addition to his Ph.D., Dr. Kim holds M.S. and B.S. in Mechanical Engineering from Seoul National University in Seoul, Korea.

Ahmad Pesaran joined NREL in 1983 and has been working on various energy systems, such as solar cooling, ocean thermal energy conversion, air conditioning, desiccant dehumidification/ cooling for buildings and buses, and most recently hybrid electric vehicles. Since 1995, he has been working on hybrid electric vehicle projects. He is currently the project manager for various activities related to battery thermal characterization, battery thermal analysis, and battery modeling and management. Dr. Pesaran holds a B.S. in chemical engineering from Shiraz University, as well as an M.S. in engineering and a Ph.D. in mechanical engineering from UCLA. He is a member of the FreedomCAR Electrochemical Energy Storage Technical Team.

© 2007 WEVA Journal, pp. 126-133